Sensor Fusion for Buried Explosive Threat Detection for Handheld Data

Mary Knox, Colin Rundel, and Leslie Collins

Duke University, Durham, NC, USA

ABSTRACT

Data from multiple sensors has been collected using a handheld system, and includes precise location information. These sensors include ground penetrating radar (GPR) and electromagnetic induction (EMI) sensors. The performance of these sensors on different mine-types varies considerably. For example, the EMI sensor is effective at locating relatively small mines with metal while the GPR sensor is able to easily detect large plastic mines. In this work, we train linear (logistic regression) and non-linear (gradient boosting decision trees) methods on the EMI and GPR data in order to improve buried explosive threat detection performance.

Keywords: ground penetrating radar, GPR, electromagnetic induction, EMI, buried threat detection, sensor fusion

1. INTRODUCTION

Worldwide, unexploded buried explosives injure and kill both adults and children. Buried explosives such as landmines or improvised explosive devices (IEDs) are indiscriminate killers in that they will maim both civilians and soldiers alike without regard to who the victim is. In 2011, landmines were responsible for the casualties of approximately 4,286 people, of which 1,320 were killed [1]. The impact of buried threats extends beyond the death toll caused by their detonation. Quality of life decreases drastically, by virtually eliminating all humanitarian efforts to areas that are known to have active buried threats; many humanitarian organizations won't allow volunteers to travel to these areas because of safety concerns [2]. Furthermore, all economic progress in an area known to contain buried threats is halted. Farming can no longer be done safely, and roads become unsafe to travel on. Thus, communities are left without consistent methods of gathering food, trading resources, and the ability to receive any sort of aid. As a result, the detection and removal of buried threats is an important goal for both military and humanitarian purposes.

Buried threats come in all different shapes and sizes, making buried threat detection difficult. The larger mines, anti-tank mines, are placed with the purpose of destroying vehicles. Smaller mines, anti-personnel mines, are buried in order to prevent enemy soldiers from passing certain areas [3]. In addition to the high variance in sizes, buried threats are made up of various materials that range from different types of metal to plastic; leading to difficulties in detection.

In this work we explore the efficacy of locating buried threats using a handheld system with electromagnetic induction (EMI) and ground penetrating radar (GPR) sensors. The performance of these sensors on different mine-types varies considerably. For example, the EMI sensor is effective at locating relatively small mines with metal while the GPR sensor is able to easily detect large plastic mines. A natural step to improving and obtaining more robust buried explosive threat detection performance is to combine information obtained from each sensor.

Previous work in using this particular handheld system improved performance after fusing EMI and GPR data [4] using a non-parametric boosting tree classifier. The classifier was trained and tested using features extracted at EMI and GPR alarm locations. The features include information extracted at the specific location, as well as the surrounding area.

Further author information: (Send correspondence to Mary Knox at Duke University)

Detection and Sensing of Mines, Explosive Objects, and Obscured Targets XXII,
edited by Steven S. Bishop, Jason C. Isaacs, Proc. of SPIE Vol. 10182, 101820D
 · doi: 10.1117/12.2263013

In this preliminary work, we explore linear and non-linear fusion algorithms, which are trained using features extracted from the handheld data at regular intervals. In order to obtain EMI and GPR information from the same location, we use thin plate splines to estimate the EMI and GPR scores throughout the lane. These EMI and GPR estimated scores are the features used in the fusion algorithms.

This paper is outlined as follows. In Section 2, we further describe the handheld data collection. In Section 3, we outline the system used to detect buried threats on the handheld dataset. In Section 4, we report the results. Finally, in Section 5, we discuss our conclusions and provide areas of future work.

2. DATA

In this work, we explore results for the handheld domain. In the typical handheld setting, a human would operate the device, swinging the detector across the lane while advancing forward along the downtrack. In this scenario, measurements would vary from run-to-run and operator-to-operator based on swing speed, speed of advance along the downtrack, height of sensor above the ground, etc.

In order to determine the capabilities of a handheld system, we consider a more controlled setting where the measurement locations are known, the swing rate is consistent, and samples are collected throughout the entire lane. This is achieved by employing a robotic cart to take GPR and EMI measurements while traveling down the lane.

Using the GPS from the cart and the sensor head position, the measurement locations are known. The robotic arm swings at a consistent rate throughout the lane. There are two GPR sensors, which are spaced 5 cm apart along the downtrack direction. The cart advances approximately 10 cm between swings. Therefore, GPR data is collected approximately every 5 cm along the downtrack. There are two EMI sensors, which are close to one another along the crosstrack direction. The EMI algorithm utilizes the difference between the two sensor responses, and the location is therefore taken to be the average of the two sensor locations.

An example path down a lane is shown in Figure 1, where each symbol represents a GPR or EMI measurement location. The GPR measurement locations are shown in blue, and the EMI measurement locations are shown in red. As demonstrated in the figure, the robotic arm on the cart swings, then the cart advances, then the arm swings again.

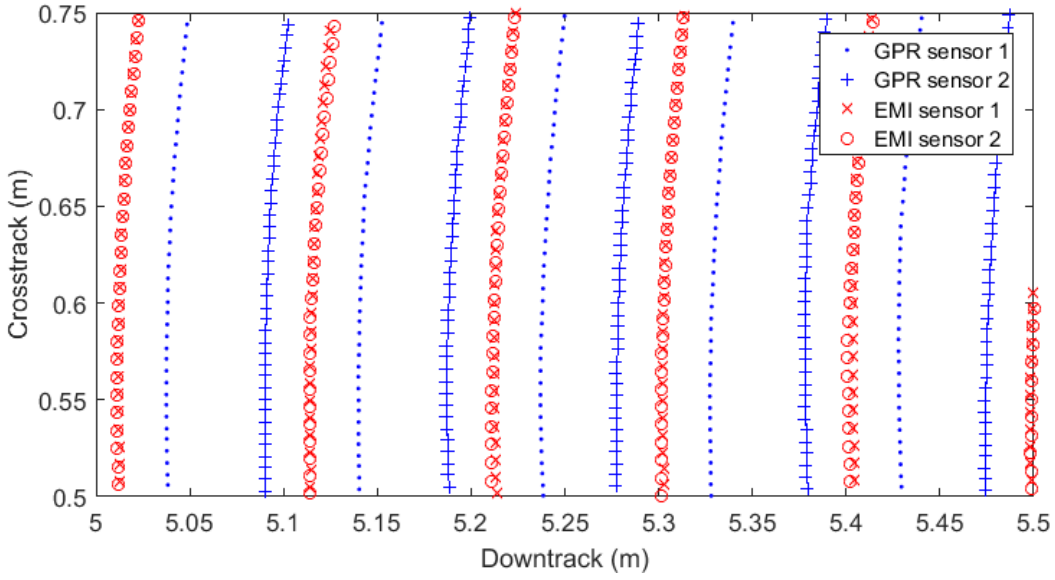

Figure 1: The GPR and EMI measurement locations are shown in blue and red, respectively. The GPR sensors are approximately 5 cm apart along the downtrack while the EMI sensors are spaced along the crosstrack.

The rate at which the robotic arm swings is much faster than the rate the cart advances. Given the samples are taken uniformly in time, there are many more samples per area during the advance than during the swing. In this work, we subsample the data such that the distance between sequential subsamples is approximately 1 cm.

The data was collected on 25 lanes (one run per lane) at an Eastern U.S. site. There are 338 targets, which consist of a wide variety of anti-tank mines, anti-personnel mines, wires, and other metallic and non-metallic clutter.

3. SYSTEM OVERVIEW

3.1 EMI PRESCREENER

Electromagnetic induction (EMI) sensors are the most common technology used in the detection of buried threats [3, 5]. Electric currents are induced in underground metal objects using a transmitter coil that emits a magnetic field. These induced currents then produce a second magnetic field. The response is then measured by the EMI sensor, and the presence of an induced field is used to detect the object [6]. EMI sensors are commonly used because they are inexpensive and perform relatively well in the detection of metallic buried threats.

We utilized the FOMIACE [7] prescreener to find targets in the EMI data. The FOMIACE precreener uses 2-D Fourier-based features in the Multiple Instance Adaptive Coherence/Cosine Estimator (MIACE) algorithm.

The Fourier features are based on the magnitudes of the 2-D FFT of a 51x21 matrix, containing the complex sine filtered [8] EMI response from 21 frequencies at 51 sequential locations. The DC component is removed and the magnitudes are scaled to be between 0 and 1.

MIACE is then trained and tested, using 25-fold cross-validation (leave one lane out), using the Fourier-based features. As the name implies, MIACE utilizes the Adaptive Coherence/Cosine Estimator (ACE) decision statistic which returns D_{ACE}, the squared cosine angle between the current observation x and the target signature s after applying background subtraction, as shown in Equation 1 where μ_b and Σ_b are the background mean and covariance respectively. The target signature is learned using a multiple instance learning method described in [9]. Finally, mean shift [10, 11] with a Gaussian kernel is used to declare alarm locations. More details regarding the FOMIACE algorithm can be found in [7].

$$D_{ACE}(x,s) = \frac{(s^T\Sigma_b^{-1}(x-\mu_b))^2}{s^T\Sigma_b^{-1}s(x-\mu_b)^T\Sigma_b^{-1}(x-\mu_b)} \tag{1}$$

3.2 GPR PRESCREENER

Ground penetrating radar (GPR) was introduced as a complementary technology to EMI [3, 12]. The GPR system takes a measurement by first emitting an electromagnetic pulse towards the ground; when a dielectric discontinuity is experienced by the pulse, it is reflected back towards the GPR sensor. A buried threat can be seen in GPR data since the buried threat creates a dielectric discontinuity between itself and the soil.

The biggest advantage in using the GPR modality over EMI is its ability to detect low-metal or non-metal targets such as improvised explosive devices (IEDs). However, it is subject to false alarms due to other dielectric discontinuities in the subsurface, such as rocks, roots, or other manmade objects.

We utilized the Histogram of Oriented Gradients - Partial Least Squares Discriminant Analysis (HOG-PLSDA) prescreener [13], which identifies landmines in GPR data using gradient based features. It is a fast method, utilizing linear classifiers.

The processing flowchart for the HOG-PLSDA prescreener is shown in Figure 2. The initial steps preprocess, or clean, the data. First, we ground align (typically to the maximum value in each A-scan [14]) and haircut (keeping the data just below the ground) the GPR data. Then, we depth normalize the data [15] by subtracting the mean and dividing by the standard deviation of the 'background' data, where the 'background' statistics are computed over nearby data that is outside of a guardband (i.e., immediate area). Each depth index is normalized independently. Since the amplitude of the received GPR signal decreases as the signal travels deeper,

depth normalization helps to standardize the GPR values over targets resulting in similar values regardless of the depth. After the data is depth normalized, we apply a median filter. In Figure 3, we show the original and the preprocessed GPR data over an anti-tank (AT) target buried at shallow and deep depths.

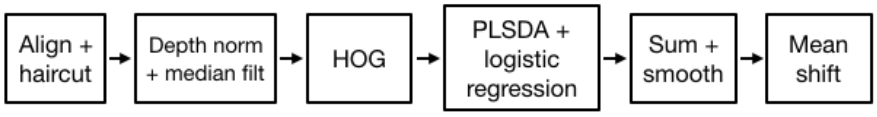

Figure 2: HOG-PLSDA prescreener flowchart.

Next, we extract HOG features on the 'cleaned' data. First, we downsample the B-scan in both dimensions by a factor of two, then compute the gradient for each pixel. We then generate a histogram, binning the gradients in a cell, in this case a 6x6 pixel region, into eight angle bins and weighting by the magnitude of the gradient. The histogram values are normalized using information from a 1x3 region of cells. The information from the normalized histograms of 3x4 cells are concatenated to form a 96-dimensional HOG feature vector.

The HOG feature vectors are then used to identify targets. We use 25-fold cross-validation (leave one lane out) to train and test PLSDA and logistic regression classifiers. We train on alarm locations, and test on all of the GPR data. The alarm locations are found using a Mahalanobis-based prescreener [16], an anomaly detector comparing the values of the current A-scan to the local statistics. These alarm locations are further fine tuned in location using the Expectation Maximization-Principal Component Analysis (EM-PCA) algorithm [17]. The EM-PCA algorithm is an iterative algorithm trained on the target examples to automatically determine the central A-scan of the target and non-target signatures. It finds the appropriate shift and polarity necessary to minimize the PCA reconstruction error by alternating between updating the PCs and finding the best central A-scan. The logistic regression values are summed over all depths and smoothed over sequential A-scans. Finally, we run mean shift with a Gaussian kernel in order to declare alarm locations.

3.3 FUSION

Data from EMI and GPR sensors has been collected in the handheld domain, and includes precise location information. The performance of these sensors on different mine-types varies considerably. For example, the EMI sensor is effective at locating small mines with metal while the GPR sensor is able to find large plastic mines. A natural step to improving and obtaining more robust performance is to combine the information obtained from each sensor.

As seen in Figure 1, the EMI and GPR measurement locations are not the same. In order to resolve the spatial misalignment of the GPR and EMI scores we used thin plate splines (TPS) [18] to continuously interpolate GPR and EMI scores throughout each lane. Thin plate splines are a penalized regression method for estimating a smooth continuous surface described by the function $f(x, y)$. This function is constructed by finding $f(x, y)$ such that it minimizes Equation 2.

$$\sum_{i=1}^{n}(z_i - f(x_i, y_i))^2 + \lambda \int\int \left(\frac{\partial^2 f}{\partial x^2}\right)^2 + 2\left(\frac{\partial^2 f}{\partial x \partial y}\right)^2 + \left(\frac{\partial^2 f}{\partial y^2}\right)^2 dydx, \tag{2}$$

Here, the first term represents a typical least squares penalty for the functions fit to the data and the second term represents a smoothness penalty. An example of the resulting TPS estimate for EMI and GPR scores is shown in Figure 4.

From Figure 4, it is clear that the EMI and GPR scores differ in target responses. As expected, different types of targets are more easily seen in one modality over the other. Also, the shape and extent of the response greatly varies between the EMI and GPR scores. More specifically, EMI scores are elevated over a greater region surrounding targets. Therefore, we extracted the TPS estimate of EMI and GPR scores over GPR score locations.

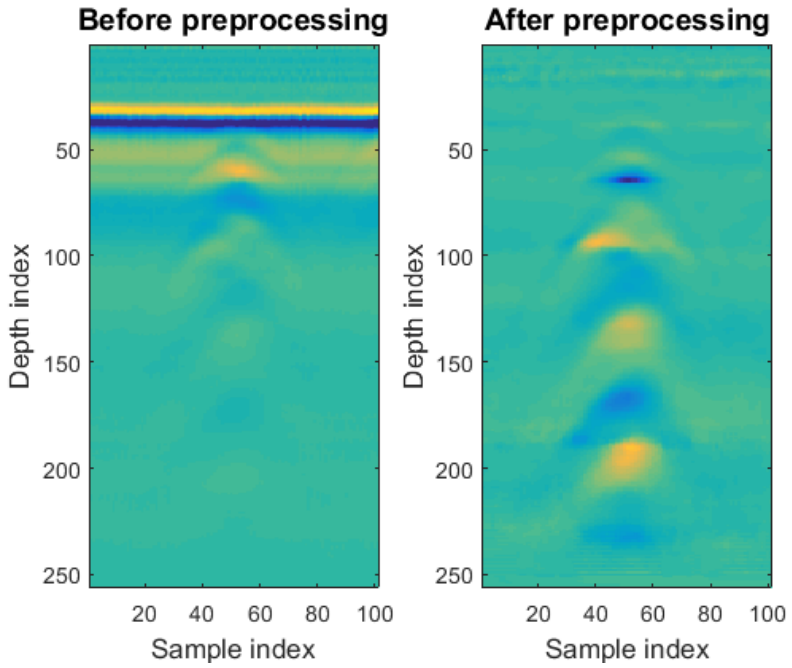

(a) Shallow anti-tank target

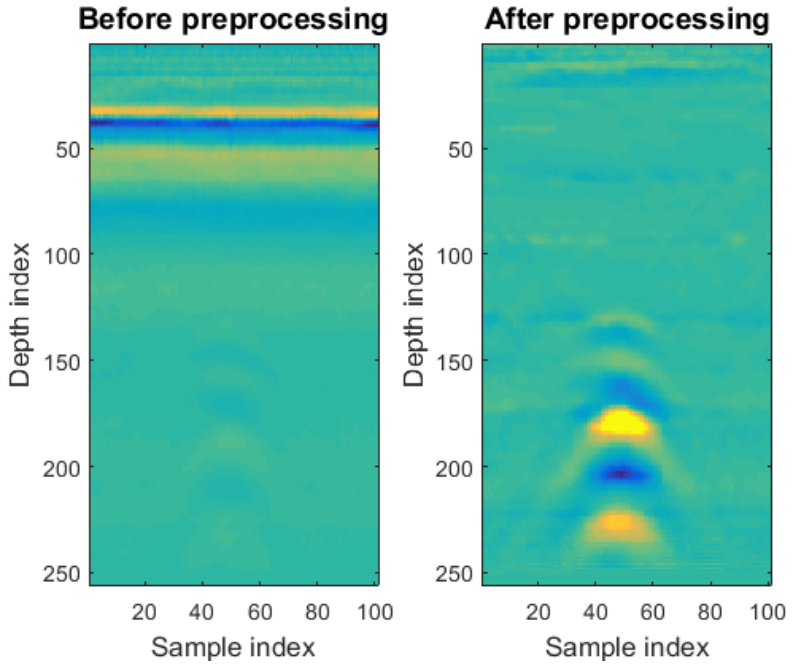

(b) Deep anti-tank target

Figure 3: GPR data over a shallow and deep anti-tank target before and after preprocessing.

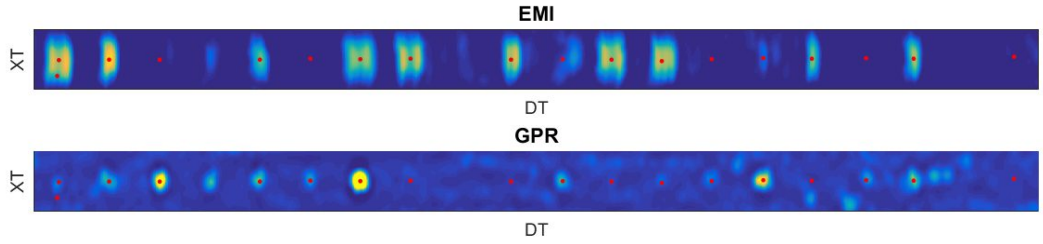

Figure 4: EMI and GPR scores for a lane. The red dots indicate buried explosive threats.

We examined two supervised methods of fusing the GPR and EMI scores: logistic regression, a linear method, and gradient boosting decision trees [19], a non-linear method. In both models we considered the TPS interpolated scores of GPR and EMI as features as well as a first order interaction. Locations within 0.25 m of a target were used as positive training examples, and all other locations were considered negative training examples. Mean shift was utilized in order to declare a reduced set of alarm locations.

4. RESULTS

The results are shown in Figure 5. We performed 25-fold cross-validation (leave one lane out) for the linear (logistic regression) and non-linear (gradient boosting decision trees) methods. For the gradient boosting approach the number of trees was varied from between 10 to 250, all of these results were similar; therefore, we only show the result when using 10 trees. Both logistic regression and gradient boosting decision trees fusion methods resulted in better performance than EMI or GPR alone. After applying mean shift, the gradient boosting fusion reported fewer alarms, limiting the extend of the ROC curve. The fusion scores for an exemplar lane are shown in Figure 6. Note that this is the same lane as was shown in Figure 4.

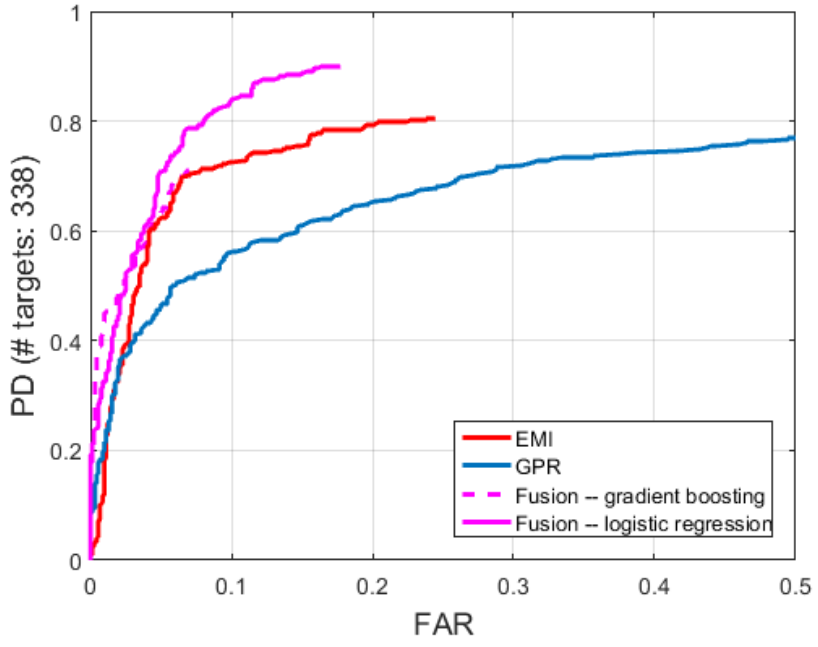

Figure 5: Receiver Operating Characteristic (ROC) curves for the EMI, GPR, and EMI/GPR fusion prescreeners.

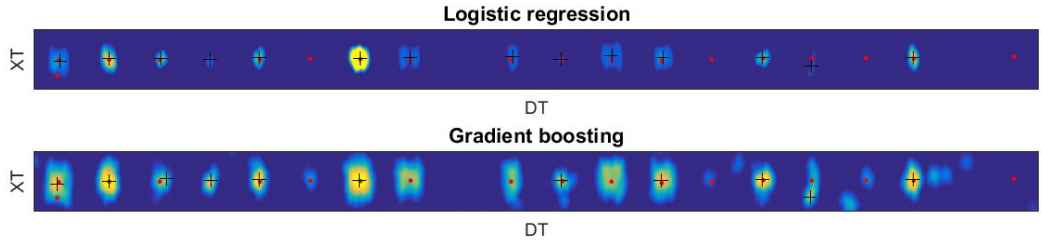

Figure 6: Fused scores for a lane. The red dots indicate buried explosive threats. The black plus signs represent alarm locations.

5. CONCLUSIONS AND FUTURE WORK

In conclusion, we present results after fusing GPR and EMI data. We investigated two fusion methods: logistic regression (a linear method) and gradient boosting decision trees (a non-linear method). Both fusion methods resulted in better performance than GPR or EMI alone. The fusion methods used as input the GPR and EMI scores for each evaluated location. We used thin plate splines to estimate the GPR and EMI scores since the GPR and EMI data was collected at different locations.

In the future, we would like to examine whether we can obtain improved results after including information from the surrounding area in addition to the information extracted at a specific location. We would also like to see how results change when changing the training/testing locations. In this work, we evaluate the system at regular intervals. However, other work examines fusion at alarm locations. It would also be interesting to examine the alarm declaration part of the system. Currently, we use mean shift to declare alarms. It could be beneficial to explore using the alarm declaration information in the algorithm training part. For example, use of an objective function to minimize the difference in area between the halos and the high scoring regions for the sensors.

ACKNOWLEDGMENTS

The authors would like to thank Dominic Ho, Alina Zare, and Brendan Alvey for sharing their GPR and EMI prescreeners. This work was supported by the U.S. Army RDECOM CERDEC Night Vision and Electronic Sensors Directorate, via a Grant Administered by the Army Research Office under Grant W911NF-14-1-0670 and Grant W911NF-13-1-0065.

REFERENCES

[1] "Landmine monitor 2012," (2012).

[2] "Mines other than anti-personnel mines," *Geneva International Centre for Humanitarian Demining* (March 2012).

[3] MacDonald, J., "Alternatives for landmine detection," tech. rep., RAND Corporation (2003).

[4] Masarik, M., Burns, J., Thelen, B., Kelly, J., and Havens, T., "Enhanced buried UXO detection via GPR/EMI data fusion," in [*SPIE: Detection and Sensing of Mines, Explosive Objects, and Obscured Targets XXI*], **9823** (2016).

[5] Bruschini, C. and Gros, B., "A survey of current sensor technology research for the detection of landmines," in [*Proc. International Workshop on Sustainable Humanitarian Demining*], **6** (1997).

[6] Won, I., Keiswetter, D., and Glenn, T., "Electromagnetic induction spectroscopy for clearing landmines," *IEEE Transactions on Geoscience and Remote Sensing* **39**(4), 703–709 (2001).

[7] Alvey, B., Zare, A., and Ho, K., "Fourier features for explosive hazard detection using a wideband electromagnetic induction sensor," *SPIE Proceedings of Detection and Sensing of Mines, Explosive Objects, and Obscured Targets* (April 2017).

[8] Scott, W., "Broadband array of electromagnetic induction sensors for detecting buried landmines," *IEEE International Geoscience and Remote Sensing Symposium* (July 2008).

[9] Zare, A., Jiao, C., and Bell, T., "Multiple instance hyperspectral target characterization," (2016).
[10] Fukunaga, K. and Hostetler, L., "The estimation of the gradient of a density function, with applications in pattern recognition," *IEEE Transactions on Information Theory* **21**, 32–40 (January 1975).
[11] Comaniciu, D. and Meer, P., "Mean shift: A robust approach toward feature space analysis," *IEEE Transactions on Pattern Analysis and Machine Intelligence* **24**, 603–619 (May 2002).
[12] Peters, L., Daniels, J., and Young, J., "Ground penetrating radar as a subsurface environmental sensing tool," *Proceedings of the IEEE* **82**, 1802–1822 (December 1994).
[13] Torrione, P., Morton, K., Sakaguchi, R., and Collins, L., "Histograms of oriented gradients for landmine detection in ground-penetrating radar data," *IEEE Transactions on Geoscience and Remote Sensing* **52**, 1539–1550 (March 2014).
[14] Knox, M., Torrione, P., Collins, L., and Morton, K., "Buried threat detection using a handheld ground penetrating radar system," *SPIE Proceedings of Detection and Sensing of Mines, Explosive Objects, and Obscured Targets XX* **9454** (May 2015).
[15] Torrione, P., Throckmorton, C., and Collins, L., "Performance of an adaptive feature-based processor for a wideband ground penetrating radar system," *IEEE Transactions on Aerospace and Electronic Systems* **42**, 644–658 (April 2006).
[16] Ho, K., Harris, S., Zare, A., and Cook, M., "Anomaly detection of subsurface objects using handheld ground-penetrating radar," *SPIE Proceedings of Detection and Sensing of Mines, Explosive Objects, and Obscured Targets XX* **9454** (May 2015).
[17] Reichman, D., Morton, K., Collins, L., and Torrione, P., "Target localization and signature extraction in gpr data using expectation-maximization and principal component analysis," *SPIE Proceedings of Detection and Sensing of Mines, Explosive Objects, and Obscured Targets XIX* **9072** (2014).
[18] Duchon, J., "Interpolation des fonctions de deux variables suivant le principe de la flexion des plaques minces," *RAIRO Analyse Numerique* **10**, 5–12 (1976).
[19] Friedman, J., "Greedy function approximation: A gradient boosting machine," *The Annals of Statistics* **29**(5), 1189–1232 (2001).